The forebrain synaptic transcriptome is organized by clocks but its proteome is driven by sleep

Noya, Sara B ; Colameo, David ; Brüning, Franziska ; Spinnler, Andrea ; Mircsof, Dennis ; Opitz, Lennart ; Mann, Matthias ; Tyagarajan, Shiva K ; Robles, Maria S ; Brown, Steven A

Abstract: Neurons have adapted mechanisms to traffic RNA and protein into distant dendritic and axonal arbors. Taking a biochemical approach, we reveal that forebrain synaptic transcript accumulation shows overwhelmingly daily rhythms, with two-thirds of synaptic transcripts showing time-of-day-dependent abundance independent of oscillations in the soma. These transcripts formed two sharp temporal and functional clusters, with transcripts preceding dawn related to metabolism and translation and those anticipating dusk related to synaptic transmission. Characterization of the synaptic proteome around the clock demonstrates the functional relevance of temporal gating for synaptic processes and energy homeostasis. Unexpectedly, sleep deprivation completely abolished proteome but not transcript oscillations. Altogether, the emerging picture is one of a circadian anticipation of messenger RNA needs in the synapse followed by translation as demanded by sleep-wake cycles.

DOI: https://doi.org/10.1126/science.aav2642

RESEARCH ARTICLE

NEUROSCIENCE

The forebrain synaptic transcriptome is organized by clocks but its proteome is driven by sleep

Sara B. Noya[1], David Colameo[1]*, Franziska Brüning[2,4], Andrea Spinnler[1], Dennis Mircsof[1], Lennart Opitz[3], Matthias Mann[4,5], Shiva Tyagarajan[1]†, Maria S. Robles[2]†, Steven A. Brown[1]†

Neurons have adapted mechanisms to traffic RNA and protein into distant dendritic and axonal arbors. Taking a biochemical approach, we reveal that forebrain synaptic transcript accumulation shows overwhelmingly daily rhythms, with two-thirds of synaptic transcripts showing time-of-day–dependent abundance independent of oscillations in the soma. These transcripts formed two sharp temporal and functional clusters, with transcripts preceding dawn related to metabolism and translation and those anticipating dusk related to synaptic transmission. Characterization of the synaptic proteome around the clock demonstrates the functional relevance of temporal gating for synaptic processes and energy homeostasis. Unexpectedly, sleep deprivation completely abolished proteome but not transcript oscillations. Altogether, the emerging picture is one of a circadian anticipation of messenger RNA needs in the synapse followed by translation as demanded by sleep-wake cycles.

A cell-autonomous circadian clock based upon feedback loops of transcription and translation functions in nearly every cell of the mammalian body and influences most aspects of physiology. In the brain, the most obvious manifestation of circadian control is the consolidation of sleep into day or night. In synchrony with sleep and wake, daily rhythmic oscillations also occur in a substantial fraction of the brain transcriptome, ranging from 3 to 4% in retina, cerebellum, brainstem, and hypothalamus, to 8 to 10% in cortex and suprachiasmatic nuclei (*1*–*4*). These oscillations are likely driven in part by rhythmic assembly and disassembly of transcription complexes and chromatin modifiers orchestrated by circadian clock–specific activators and repressors such as BMAL1/NPAS1, PERIOD (PER1 and PER2), and CRYPTOCHROME (CRY1 and CRY2), as observed in other tissues (*5*–*8*). However, it has become increasingly apparent that posttranscriptional processes play an important role in circadian regulation. In liver and suprachiasmatic nuclei (SCN), the best-studied circadian tissues to date, evidence of circadian mRNA processing, polyadenylation, and translation have appeared (*9*–*11*). Complicating matters still further, circadian oscillations in mRNA levels can also be driven by temporally consolidated behaviors. In liver, timing of food intake contributes to rhythmic transcription (*12*), and in cortex, sleep-wake cycles play a major role (*3*).

Relative to all other cell types, neurons present a special case because mRNA is distributed to potentially distant compartments such as axonal terminals and postsynaptic spines. Although the axodendritic arbor contains only ~10% of total transcripts (*13*), a large literature demonstrates that mRNAs are actively transported to neurites (*14*–*16*). Downstream, local synaptic translation of mRNA has been postulated to be an important mechanism in memory (*17*, *18*), and both synaptic size and total protein abundance are dynamically scaled by wake and sleep (*19*, *20*).

Despite this context, circadian and sleep-wake–dependent regulation of synaptic transcript pools in brain, as well as their functional importance, remain entirely unexplored questions. "Multi-omic" approaches have been increasingly used to understand complex questions of cellular regulation, and therefore might also be useful to explore the connectivity between the clockwork and sleep (*21*). Here, we used a combination of biochemical fractionation, deep sequencing, single-transcript confocal microscopy, and mass spectrometry (MS)–based quantitative proteomics to analyze the origin and function of rhythmic daily oscillations in the transcripts and proteins of forebrain synapses. From these studies, we derive the simple paradigm that a clock-gene–dependent mechanism is needed to provision synapses with mRNAs in a circadian fashion, which are then translated in response to sleep-wake cycles.

[1]Institute of Pharmacology and Toxicology, University of Zürich, Zurich, Switzerland. [2]Institute of Medical Psychology, LMU Munich, Germany. [3]Functional Genomics Center Zurich, University of Zurich–Eidgenosissche Technische Hochschule, Zurich, Switzerland. [4]Department of Proteomics and Signal Transduction, Max Planck Institute of Biochemistry, Martinsried, Germany. [5]Clinical Proteomics Group, Proteomics Program, Novo Nordisk Foundation Center for Protein Research, University of Copenhagen, Copenhagen, Denmark.
*Present address: Laboratory of Systems Neuroscience, Department of Health Science and Technology, Institute for Neuroscience, Swiss Federal Institute of Technology, Zurich, Switzerland.
†Corresponding author. Email: steven.brown@pharma.uzh.ch (S.A.B.); charo.robles@med.uni-muenchen.de (M.S.R.); tyagarajan@pharma.uzh.ch (S.T.)

The forebrain synaptic transcriptome shows pervasive daily rhythmicity

To generate a time-resolved map of the synaptic transcriptome from the mouse forebrain, we purified synaptoneurosomes using biochemical fractionation with discontinuous Percoll gradients (*22*). Synaptoneurosomes represent axonal nerve terminals (cytoplasm, synaptic vesicles, mitochondria, and cytoskeleton) and attached postsynaptic structures. We collected forebrains every 4 hours across the day in biological triplicates under natural conditions of light and dark (LD), and identified mRNAs by high-throughput sequencing in the forebrain homogenates and the purified synaptoneurosomes (Fig. 1A). After normalization and thresholding (see materials and methods), we detected 14073 unique transcripts. These transcripts overlapped almost completely with those identified in the hippocampal neuropil (*23*), a highly projection-enriched brain region (Fig. 1B), as well as with other similar transcriptomes of forebrain synapses (*24*) (fig. S1A). In addition, quantitative polymerase chain reaction demonstrated enrichment of known synaptic mRNAs and depletion of nuclear ones (fig. S1B). These measures confirmed the validity of our biochemical approach. Reasoning that a fold change of ≥1.5 in synaptic versus forebrain abundance should represent a reasonable criterion with which to identify a specific synaptic element, we found 3104 unique synaptically enriched mRNAs (Fig. 1B and table S1). Gene Ontology (GO) analysis corroborated the overwhelming predominance of synaptic annotations among these transcripts, as well as their stepwise enrichment across the analytical steps of the procedure (Fig. 1C).

Using the Perseus computational platform (*25*), we analyzed these synaptically enriched mRNAs for evidence of daily rhythmicity (period 24 hours, $q < 0.05$), and found that 2085 (67%) were cycling, the highest proportion of rhythmic transcripts estimated in any tissue, cell, or organelle described to date (Fig. 1D and table S2; results with other q-value cutoffs are shown in fig. S1C). The average fold change was 1.8 (Fig. 1E) and the majority showed a peak-trough amplitude of 1.5 or greater (fig. S1D). The 2085 cycling features overlapped substantially with those detected using other algorithms (91% with the JTK_CYCLE algorithm; period 24 hours, $q < 0.05$) (*26*) (fig. S2A). In parallel, we analyzed the forebrain transcriptome and found that only 6% of it was oscillating (Fig. 1F, fig. S2B, and table S3). Notably, 93% of synaptic circadian transcripts were cycling exclusively in the synapse; only 7% were cycling also in the whole forebrain and with reduced amplitudes (Fig. 1G and fig. S2C). This minimal overlap implies that daily oscillations

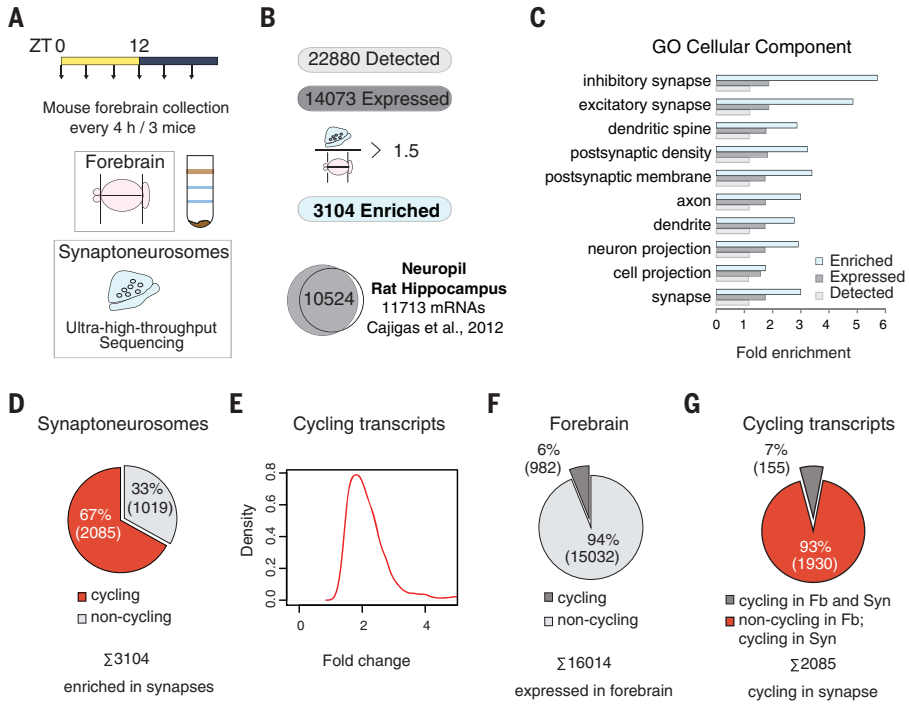

Fig. 1. Daily rhythms within the synaptic transcriptome. (**A**) Workflow: Forebrains from mice were collected in biological triplicates at six times throughout the day. Synaptoneurosomes were prepared, RNA isolated and sequenced, and data analysis was performed using Perseus software. (**B**) Number of transcripts from successive steps of the synaptoneurosome workflow. Synaptic transcripts were those 1.5-fold enriched in synapses versus total forebrain. Right: Detected transcripts correspond closely to those identified in synaptic neuropil (*23*). (**C**) Top 10 GO cellular component annotations. BH-adjusted $p < 0.001$, FunRich analysis (http://www.funrich.org) in the synaptic transcriptome. Bars show the calculated fold enrichment versus the mouse genome for synaptic-enriched (blue), detected (light gray), and expressed (dark gray) GO-associated transcripts. (**D**) Pie chart depicting the fraction of cycling mRNAs (Perseus time-series periodic analysis, period 24 hours, $q < 0.05$) among enriched synaptic mRNAs. (**E**) Density distribution of circadian amplitudes (peak/trough) of cycling synaptic transcripts from (D). (**F**) Fraction of cycling mRNAs (Perseus time-series periodic analysis, period 24 hours, $q < 0.05$) in the whole forebrain. (**G**) Comparison of synaptic-enriched circadian RNAs in synaptoneurosomes versus total forebrain. Note that, of the synaptic cycling mRNAs ($n = 2085$), only 7% ($n = 155$) cycle in the forebrain and the synapse (gray) and 93% ($n = 1930$) cycle exclusively in synapses.

in the synaptic transcriptome are entirely or nearly entirely driven by posttranscriptional processes.

In principle, oscillations in the abundance of synaptic transcripts could arise either from transport of mRNAs or from local control of their stability. Both to verify our transcriptional results and to distinguish between these possibilities, we employed single-mRNA fluorescence in situ hybridization (FISH) using the mRNAscope strategy (see materials and methods). As test cases, we selected the vesicular glutamate transporter *Slc17a7* (vesicular glutamate transporter 1) and *Lingo1* (leucine rich repeat and Ig domain containing 1), with previously reported synaptic function, high levels of expression in hippocampal cornu ammonis area 1 (CA1) and cortex (*27*, *28*), and high amplitude in our circadian analysis. As a control, the circadian clock mRNA *Cry1* was also imaged. F2

Using custom automated imaging workflows (see materials and methods), we visualized and quantified axodendritic and somatic mRNAs separately in hundreds of images. Similar to previous reports (*29*), *Cry1* mRNA in the hippocampus increased toward the end of the dark period, and the same trend was observed in the cortex (fig. S3, A and B). For synaptic cycling mRNAs, robust oscillations were observed in the axodendritic compartment (Fig. 2A and fig. S4), with maximum levels at Zeitgeber time (ZT) 4 and trough levels at ZT12 in both CA1 and cortex (Fig. 2B). We further quantified CA1 dendritic structures according to distance from the pyramidal cell layer. Equal daily rhythms of mRNA abundance were observed at all distances (Fig. 2C). Even though synaptic density dramatically increases with distance (*30*), we found identical circadian amplitude at all distances, suggesting that the synaptic oscillations of transcript abundance are likely generated through transport along the dendritic arbor. However, other explanations such as regulated RNA stability certainly also remain possible.

Synaptic oscillations anticipate dawn and dusk and depend on a functional clock

Cycling synaptic transcripts clustered entirely into two temporal categories, with maxima anticipating dawn or dusk (lights-on and lights-off in our laboratory scenario; Fig. 3A). Because these peaks of transcript accumulation anticipated light-dark transitions, we hypothesized that they were driven by a circadian clock. To verify this presumption, we did synaptoneurosome transcriptome analysis at two time points (ZT0 and ZT12) from mice kept in normal LD conditions, mice kept in constant darkness, or *Bmal1*-knockout mice ($Bmal1^{-/-}$), which lack an essential clock gene and therefore lack a functional circadian oscillator (*31*). Transcripts showing significant differences in abundance [exact binomial test, Benjamini–Hochberg (BH)-corrected $p < 0.05$] between the two times in wild-type mice under LD conditions (Fig. 3B; significant values are shown in red) also showed differences when kept in darkness (Fig. 3C; significant values are shown in dark gray). Conversely, no significant changes were observed for those transcripts in $Bmal1^{-/-}$ mice (Fig. 3C; significant values are shown in green). F3

The two waves of transcript abundance that we detected were not only sharply segregated by phase, but were also entirely ontologically distinct (Fig. 4, A and B; fig. S5; and table S4). Moreover, the light and dark circadian synaptic clusters were further enriched in specific biological processes compared with the whole synaptic transcriptome (fig. S5 and table S4), emphasizing an important temporal and local regulation. mRNAs anticipating dusk participate in cellular pathways related to synapse organization, synaptic transmission, and higher functions relying on them directly, such as memory, learning, and behavioral outputs (Fig. 4A). Those anticipating dawn are required for metabolism, with a high representation of lipid catabolism, translation, and cell proliferation or development (Fig. 4B). F4

Coordination of daily mRNA oscillations by circadian clocks and sleep cycles

The major behavioral output of the circadian oscillator in brain is the sleep-wake cycle. At the level of the whole forebrain, it has been demonstrated previously that the vast majority of "circadian" transcription is actually sleep-wake driven (*3*). To arrive at this conclusion, the authors systematically deprived mice of sleep for the 6 hours preceding sacrifice at four different times of day during the circadian cycle, thereby keeping sleep pressure high across all samples (*3*, *32*). By so doing, they observed that circadian oscillations of most brain transcripts

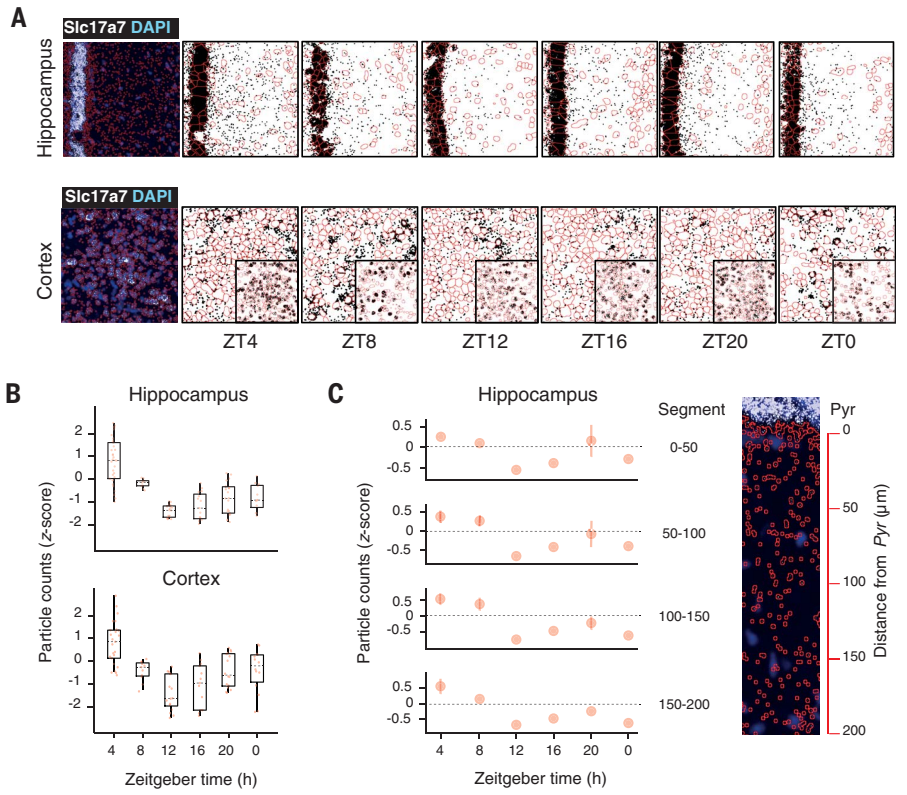

Fig. 2. mRNA FISH visualization of Slc17a7 (VGlut1) diurnal abundance in hippocampus and cortex. (**A**) Confirmation of rhythmicity by single-molecule fluorescence in situ hybridization (FISH) of *Slc17a7* (*VGlut1*) in the stratum radiatum of the CA1 of the hippocampus (top panels) and in the axodendritic compartment of cortex (lower panels). For better visualization, red line traces nuclei and single mRNA dots are increased to 0.5 µm. Insets: mRNA in the somatic areas of the cortex. (**B**) Quantification of mRNA abundances in (A) (n = 13 to 18 from three biological replicates). (**C**) Quantification of mRNA in stratum radiatum normalized and plotted as a function of distance from the pyramidale (Pyr) segments. Sample image is shown at right (mean ± SD).

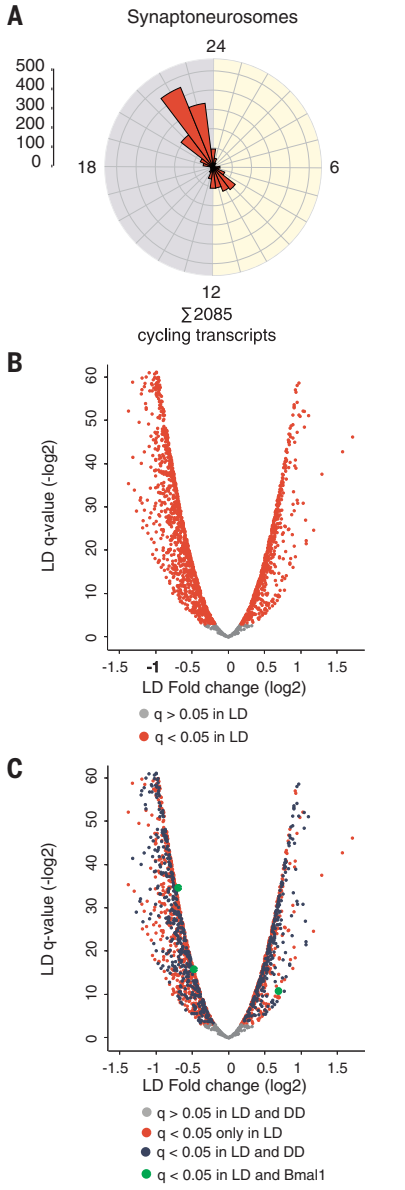

Fig. 3. Synaptic RNA abundance anticipates dawn and dusk and depends on a functional circadian clock. (**A**) Phase distribution of the rhythmic synaptic transcriptome in LD. Angular axis, Zeitgeber time; magnitude, number of transcripts peaking at indicated time. (**B**) Volcano plot representing the fold change and q value between ZT0 and ZT12 for the total synaptic rhythmic transcriptome from mice kept under LD conditions (12:12). Red dots, mRNAs with abundance significantly different between times (t test, $q < 0.05$, n = 3); gray dots, mRNAs not significantly different. (**C**) Volcano plot as in (B), where mRNAs are labeled as follows: red, significant differences between ZT0 and ZT12 only (i.e., in LD conditions only); blue, significant differences between CT0 and CT12 as well (i.e., after 48 hours of dark:dark conditions); green, significant differences between the same time points in *Bmal1*$^{-/-}$ clock-deficient mice after 48 hours of dark:dark conditions. For visualization purposes, the three significant dots were enlarged (n = 3).

disappeared. To test whether synaptic mRNA oscillations are controlled by sleep pressure, we first derived an analogous protocol in which sleep pressure would be kept elevated across the circadian day at levels roughly equal to its normal 24-hour maximum under undisturbed conditions. Typically, sleep pressure is indicated by the amplitude of subsequent electroencephalogram (EEG) oscillations during sleep: the greater the sleep pressure, the greater the amplitude of "delta" oscillations (0.5 to 4 Hz) (*32*). As can be seen in Fig. 5, A and B, across six equally spaced time points during the day, 4 hours of prior sleep deprivation by gentle handling leaves at each time point a level of delta power approximating that maximally observed spontaneously in the day before the manipulation (top lines), without disrupting the circadian phase of sleep-wake behavior the following day (bottom lines). Although some fluctuation in delta power across time points is still observed, we estimate it to be less than one-fifth of that observed under the same conditions across the normal circadian day. At some times of day (e.g., the start of the day at ZT0 to ZT4, when mice are sleeping; fig. S6, A and B), this sleep deprivation results in a significant decrease in sleep latency (the time to fall asleep, fig. S6C) and increase in delta power (Fig. 5, A and B) relative to control conditions. At other times (e.g., the start of the night at ZT12 to ZT16, when mice would normally be awake anyway; fig. S6, A and B), the same sleep deprivation results in almost no changes relative to control conditions (Fig. 5, A and B, and fig. S6, C and D). In all cases, subsequent sleep and activity are completely normal, with no shift in the timing of activity (Fig. 5, A and B).

We next performed this protocol preceding each time point of our synaptoneurosome transcriptomics (Fig. 5, A and B). Consistent with observations of the whole-brain transcriptome by other investigators (*3*), the rhythmicity of a large proportion of mRNAs in synaptoneurosomes was significantly altered by sleep deprivation. In general, cycling features in baseline (BL) conditions showed reduced statistical significance (higher q values) under sleep deprivation (SD) (Fig. 5C and table S5). However, circadian oscillations of one-fourth (561) of

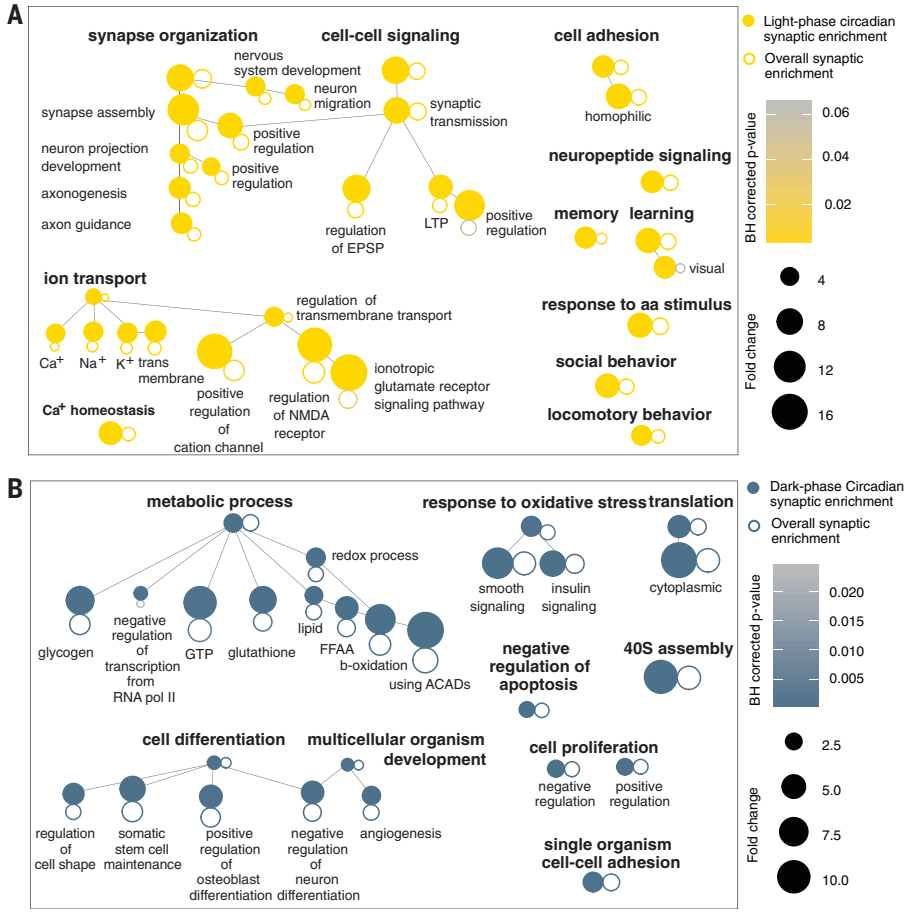

Fig. 4. Predawn and predusk mRNAs relate to specific and distinct functions. (**A**) GO analysis of biological processes enriched in the light (predusk) mRNA cluster (725 genes), grouped according to ontological hierarchy. Circle size is proportional to the fold enrichment and color is proportional to significance. Higher-level annotations are in bold. BH-corrected $p < 0.001$, FunRich analysis (http://www.funrich.org). Open circles, enrichment for the same terms in the overall synaptic transcriptome. (Note the decrease in fold enrichment and significance for most annotations.) (**B**) Same as in (A), but for the dark peaking (predawn) mRNA cluster ($n = 1217$ genes).

synaptic mRNAs were preserved (period 24 hours, $q < 0.05$) and virtually unchanged in amplitude compared with BL conditions (Fig. 5, D to F, and fig. S7A), and of the remaining 1524 transcripts, 1271 still showed profiles with considerable time-of-day–dependent variation (Fig. 5G and fig. S7B). Ontologically, the analysis of rhythmic mRNAs presents a picture that is mostly unchanged (table S6). mRNAs that encode proteins involved in synaptic transmission are enriched in the peak before the transitions to the wake phase (Fig. 6A). By contrast, mRNAs peaking before dawn, preceding the sleep phase, are involved in intracellular signaling, cell morphology, cell metabolism, and translation (Fig. 6B).

Daily variations in the synaptic proteome are dominated by sleep-wake state

Previous studies suggested that mRNAs in the synapse are translated there, and half of these locally translated transcripts were also present in our cycling dataset (*24*) (fig. S8). To gain further insights into the functional implication of daily oscillations of synaptic mRNAs, we performed MS-based, label-free quantitative proteomics to characterize temporal patterns of the total forebrain and synaptic proteome. We measured, in a single-shot manner, protein samples prepared from isolated synaptoneurosomes and total forebrain of mice (four biological replicates) collected every 4 hours across 24 hours (see materials and methods). Our in-depth analysis allowed us to quantify across all samples 4477 proteins in total forebrain and 4063 in synapses, with an overlap of 3710 proteins (fig. S9A). Circadian analysis revealed that in synapses, 11.7% of proteins (476; Fig. 7A and table S7A) and in total forebrain, 17.2% of proteins (770; fig. S9B) were rhythmic (period 24 hours, $q < 0.1$; table S7B). [Note that proteomic analyses showed lower circadian range and relative signal for less abundant components than transcriptomics; the q value was set at 0.1 at the maximum of the circadian q-value distribution to ensure comparable coverage and comparability with transcriptomics (fig. S9, C and D). Analyses identical to those in Fig. 7 are also presented in fig. S10, with a q value set at 0.05, arriving at the same conclusions with smaller numbers of proteins.]

Although both the cycling synaptic and forebrain proteomes showed biphasic distributions, these were markedly different (fig. S11, A and B, and table S7C), with peak phases differing across compartments by 6 hours (fig. S11, C and D). Moreover, from the common proteins in both datasets (fig. S9A), only 92 were cycling in both forebrain and synapse, and these also had substantially different phases of maximal expression (Fig. 7, B and C, and fig. S11, E and F), suggesting, as for the transcriptome, totally different mechanisms for daily protein rhythm generation in the two compartments.

By contrast, the phase distribution of synaptic cycling proteins mirrored that observed for oscillating synaptic transcripts, with two clusters preceding dusk and dawn (fig. S11, B and D). We detected synaptic mRNAs for 1128 synaptic proteins (fig. S12A) and, of those with daily oscillations (fig. S12B), 77.7% also had a cycling transcript predominantly with a leading or sharing phase (Fig. 7, D and E). As revealed for transcripts, proteins peaking before dawn were enriched in categories related to metabolism, and more specifically to lipid metabolism and mitochondria, whereas proteins involved in cellular signaling preceded dusk (Fig. 7, F and G, and table S8). Thus, under normal conditions of light and dark, the temporal profiles of the synaptic proteome largely resembled those of the transcriptome.

Analogously to the transcriptome, we next examined the daily cycles in the proteome under conditions of high sleep pressure. Here, a markedly different picture emerged. In the time course from the serial sleep deprivation, almost all (98% with a cutoff of $q < 0.1$ and 99.9% with a cutoff of $q < 0.05$) of the oscillating proteins in BL lost their rhythms (period 24 hours, $q < 0.1$; Fig. 8, A to C, and table S9). Our data indicate that daily changes in protein levels at the synapse are completely determined by vigilance state rather than by circadian clocks.

Discussion

In various mammalian tissues, between 3 and 16% of total transcripts have been described as circadian until recently (*33*), and our own figure of 6% of oscillatory mRNAs in the whole mouse forebrain is consistent with these values. However, synaptic functionality has been shown to have a strong circadian component. In the hippocampus, long-term potentiation efficacy undergoes circadian variation (*34*), and in the SCN, dynamic expression and function of ion

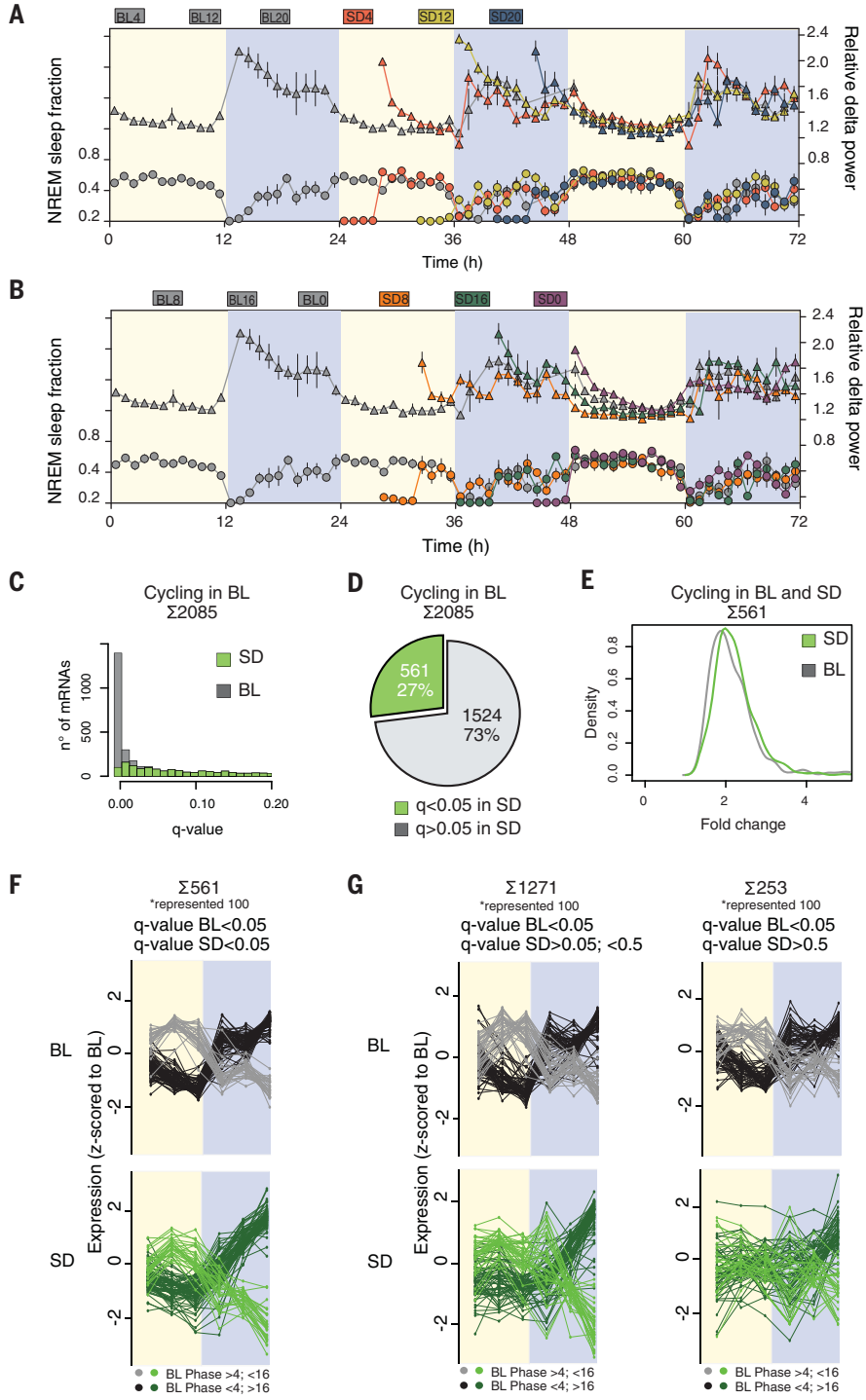

Fig. 5. Circadian and sleep-wake regulation of synaptic mRNA abundance. (**A**) and (**B**) Mean (±SEM) time course of EEG relative (to mean BL delta power; 0.5 to 4 Hz at ZT8 to ZT12) frontal delta power during NREM sleep (triangles; percentage of the last 4 hours of the BL light periods) and time spent in NREM sleep (circles; minutes/recording hours; left *y*-axis) during 24 hours of BL (gray symbols and lines), 24 hours of recovery, and during and after 4-hour SD finishing at ZT4 (red, sample name BL4/SD4), ZT8 (orange, sample name BL8/SD8), ZT12 (yellow, sample name BL12/SD12), ZT16 (green, sample name BL16/SD16), ZT20 (blue, sample name BL20/SD20), or ZT0 (purple, sample name BL0/SD0). Gray areas delineate the dark periods. The data was divided into two panels for better visualization but the baseline is the same in both. (**C**) Distribution of *q* values (Perseus time-series periodic analysis, period 24 hours) of the 2085 mRNAs cycling in BL (in red are *q* values at BL, in green are *q* values after SD). *q* values > 0.5 were omitted. (**D**) Pie chart depicting the fraction of mRNAs that remain rhythmic (Perseus time-series periodic analysis, period 24 hours, $q < 0.05$) in synaptoneurosomes of SD mice. (**E**) Density distribution of circadian amplitudes (peak/trough) of cycling synaptic transcripts that remain rhythmic after SD. In gray is the amplitude in BL and in green the amplitude in SD. (**F**) Expression profiles of transcripts cycling in BL and SD (*q*-value BL < 0.05 and *q*-value SD < 0.05; 561 mRNAs). One hundred randomly selected mRNAs are shown. (**G**) As in (F), but for those transcripts cycling in BL ($q < 0.05$) but nonsignificant in SD; $n = 1271$ transcripts with lower *q* values in SD ($0.05 < q < 0.5$; left) and $n = 253$ transcripts with higher *q* values in BL ($q > 0.5$; right) are represented separately. One hundred randomly selected mRNAs are shown.

channels or neurotransmitter receptors ensure distinct effects of light depending on time of day (*4*, *35*–*37*). Helping to achieve this circadian functionality, we find that synaptic transcript accumulation can occur with much higher rhythmicity: 67% of enriched synaptoneurosomal transcripts show time-of-day variation, encompassing all aspects of synaptic function. (It should be noted that other transcripts present but not specifically enriched at synapses do not display this overwhelming degree of rhythmicity, implying differences in stability, circadian active transport, or both.)

Posttranscriptional mechanisms as a primary circadian motor

Statistically, our results further show that this rhythmicity is generated at a posttranscriptional level, because overlap between the set of synaptic cycling transcripts and that in the whole forebrain is at levels expected by chance alone. This observation is consistent with several recent studies showing circadian variation at steps subsequent to transcription initiation (*10*, *11*, *38*–*40*). In the brain, we observe rhythms of transcript abundance microscopically at equal amplitude throughout the axodendritic arbor in the stratum radiatum of the hippocampus despite marked variation in synaptic density. Thus, spine-poor proximal regions (*30*) show the same amplitude

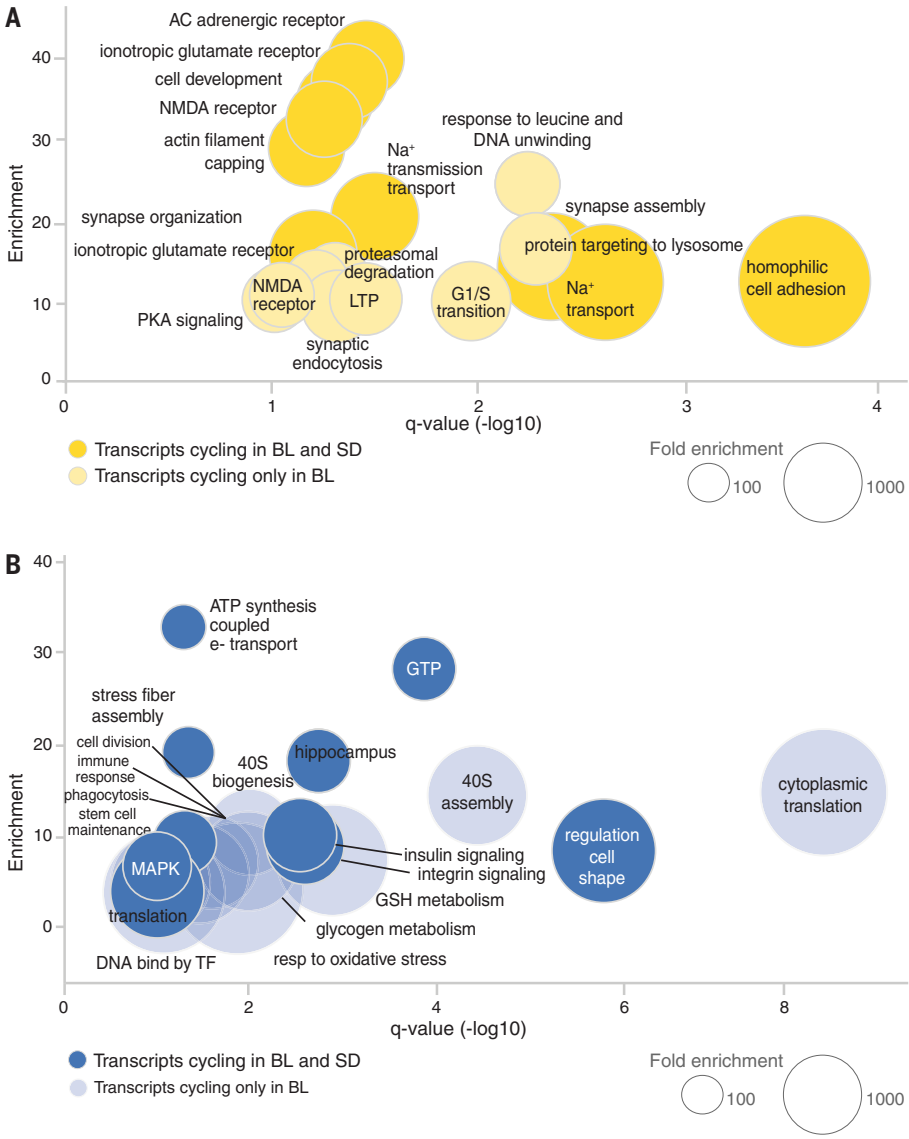

Fig. 6. Synaptic accumulation of RNA preceding dawn and dusk is independent of sleep pressure. (**A**) GO analysis of biological processes enriched in the light (predusk) peak (according to phase in BL). In dark yellow are transcripts cycling in both BL and SD; in light yellow are those cycling significantly in BL but nonsignificantly in SD (light yellow). Size of the circle indicates fold enrichment in the light versus dark. (**B**) Same as in (A), but for the dark peak, with circle size indicating enrichment in dark versus light.

as spine-rich distal regions. For this reason, we favor the hypothesis that the generation of synaptic transcript daily oscillations happens owing to cyclical transport to synapses. Dynamics of cytoskeleton components have already been linked to the circadian clock (*39*, *40*) and represent a possible regulatory node for transport in the cytoplasm. However, other interesting posttranscriptional steps could be involved, including changes in the RNA degradation rate within the dendritic arbor or at synapses. Because messenger ribonucleoproteins remain docked at the nuclear basket for an uncertain time, constituting a rate-limiting step for mRNA dynamics (*41*, *42*), export through the nuclear pore is also an appealing regulatory step for circadian regulation of mRNA abundance outside the nucleus.

A similar lack of parallelism between synapse and whole forebrain can be observed when examining the proteome. Three-quarters of cycling synaptic proteins arise from cycling synaptic transcripts, but only 20% of proteins show oscillations in the whole brain. It is difficult to draw conclusions about the relative percentages of oscillatory transcripts and proteins because different platforms were used for data generation (deep sequencing versus mass spectrometry). However, our results are consistent with the reported stability of many synaptic proteins (*19*), which would correspondingly decrease their oscillatory amplitude. There is also a small difference in overall phase angle between the two datasets. This phase discrepancy suggests that local translation of synaptic proteins could be a major rate-limiting step for daily changes in synaptic protein levels. Supporting this idea, a recent study in neuronal culture demonstrates that mRNA localization in the synapse is the primary mechanism contributing to the synaptic proteome compared with transport of proteins synthesized in the soma (*43*).

A major division of biological functions preparing for sleep and wake

In most mammalian organs, broad peaks of gene expression precede dusk and dawn (*2*). In our own study, nearly without exception, both circadian transcripts and the proteins derived from them showed peak levels sharply in anticipation of dusk and dawn. Transcripts in these two phases showed a complete division of biological function: cell-intrinsic and metabolic ontological terms preceded sleep, whereas terms associated with synaptic structure and function preceded wake. The division that we observed is consistent with a large literature suggesting both circadian- and sleep-dependent partition of cellular function. An inherent circadian clock is known to regulate learning and memory efficiencies diurnally (*44*–*47*). Mechanistically, it has being proposed that trafficking of glutamate receptors or modulation of spine densities could be involved (*48*–*50*). Along the same lines, synaptic homeostasis has been proposed as a major function of sleep-wake states (*20*), and others have proposed macromolecular synthesis and energy replenishment as potential functions for sleep (*51*, *52*). Our synaptic GO data are consistent with both suggested functions of sleep-wake cycles, neatly partitioned in circadian time. In a companion paper (*53*), we further document the role of synaptic protein phosphorylation across the circadian cycle. Again, we found a purely bimodal distribution of these ontological states, though with opposite relative proportions: whereas the majority of cycling RNAs and proteins reach peak levels at the end of the wake period in anticipation of day, the majority of circadian phosphosites reach peak levels at the end of the sleep period in anticipation of dusk (*53*).

Transcript timing is dominated by clocks, protein timing by sleep-wake state

Because of the coupling of circadian rhythms and sleep-wake cycles, distinguishing the contribution of each to cellular biology remains challenging. By depriving mice of sleep before each time point, one mostly dampens the normal diurnal variation of sleep need: during the light phase, SD induces an increase in sleep pressure, whereas during the dark phase, no significant

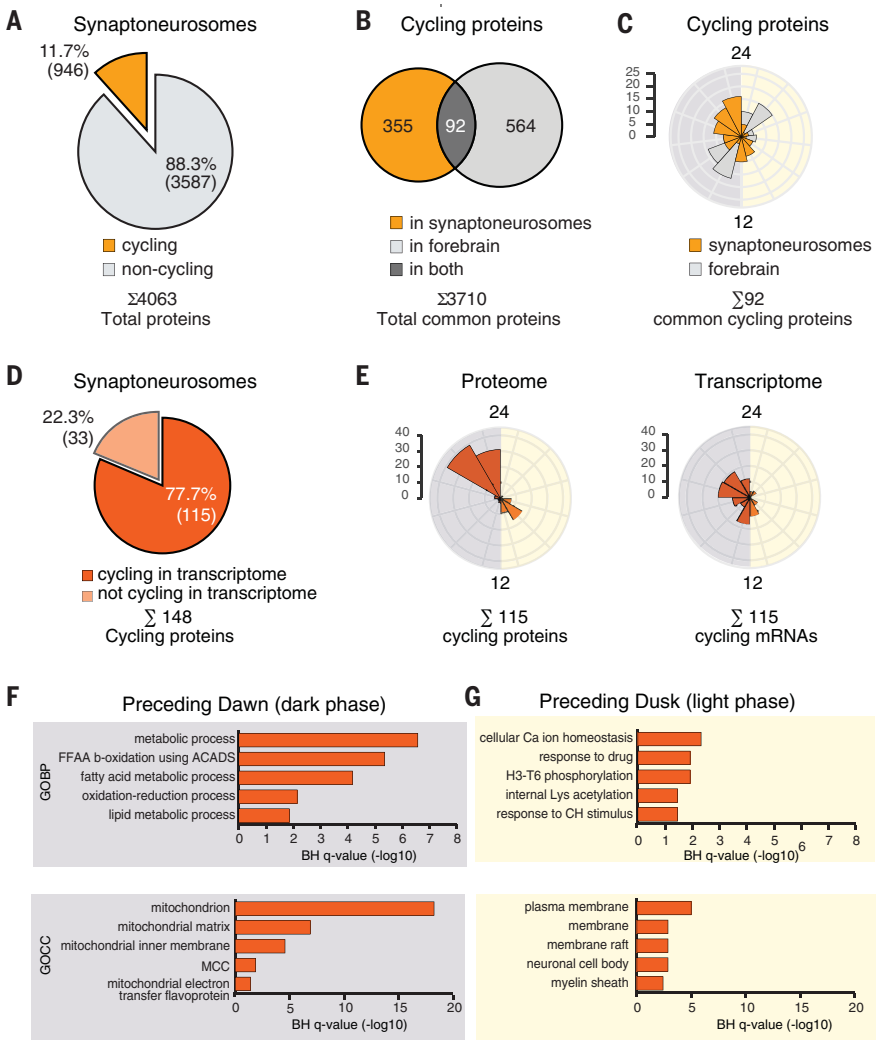

Fig. 7. Oscillations of the synaptic proteome resemble those of the synaptic transcriptome. (**A**) Pie chart showing the fraction of cycling proteins (Perseus time-series periodic analysis, period 24 hours, $q < 0.1$) in synaptoneurosomes among the total 4063 quantified. (**B**) Overlap of the rhythmic proteome in synapses and in total forebrain from those quantified in both compartments ($n = 3710$ proteins). (**C**) Phase distribution in synapses (orange) and forebrain (gray) of proteins cycling in both compartments. (**D**) Proportion of synaptic cycling proteins with synaptic cycling mRNAs. (**E**) Rose plots representing the frequency distribution of phases for cycling proteins and corresponding transcripts at synapses. (**F** and **G**) Enriched GO Biological Processes (GOBP) and GO Cellular Components (GOCC) in the cycling synaptic proteome, with cycling transcripts separated according to protein phase: dark, anticipating dawn (F) and light, and anticipating dusk (G). BH-corrected $p < 0.01$, FunRich analysis (http://www.funrich.org).

difference occurs because animals are already awake (Fig. 5A and fig. S6) (*32*). Under these conditions, circadian transcriptional oscillations of the mouse forebrain are strongly dampened (*3*). At the synapse, the posttranscriptional mechanisms dominating diurnal transcript accumulation are less affected: whereas circadian rhythmicity is globally decreased, one-fourth of circadian transcripts remain completely unchanged, and most others retain some evidence of time-dependent variation.

These time-of-day–dependent oscillations in synaptic transcript abundance persist in constant darkness, ruling out light-driven effects, but are lost in circadian clock–deficient *Bmal1*$^{-/-}$ mice in entrained LD conditions. It is thus tempting to attribute cyclical abundance purely to circadian clock control. However, *Bmal1*$^{-/-}$ mice (*54*), as well as all other clock-depleted strains tested (*55*), show markedly dampened daily variation in sleep pressure across the day, even under normal LD conditions. Therefore, our experiments do not rule out clock:sleep interactions, even if they demonstrate total dependence of cyclic synaptic RNA accumulation upon clock function.

Ontological terms related to synaptic organization and assembly, cell adhesion, and actin cytoskeleton all retain high statistical significance and synaptic enrichment equally under conditions of sleep deprivation. Thus, sleep-wake cycle–dependent changes in synaptic structure (*20*, *56*, *57*) appear to be preceded by a primarily circadian-driven accumulation of relevant RNAs.

At the protein level, almost no circadian influence remains under conditions of high sleep pressure. Although daily cycles of proteins in the synapse are detected in animals kept under an LD cycle, sleep deprivation completely blunts those changes.

Our findings are consistent with cellular literature suggesting activity-dependent translation at synapses: new experience triggers the association of mRNAs to ribosomes in the synapse, synaptic activation rapidly releases the translational repression of mRNAs localized in the synapse, and local protein translation is essential for several forms of plasticity that involve active behavior (*58*–*61*). Similarly, evidence of synaptic downscaling during sleep has been observed ultrastructurally in mouse cortex (*56*) and likely occurs because of metabotropic glutamate receptor 5 (mGluR5)–dependent signaling during waking (*19*). Thus, under the serial SD protocol that we used, as oscillations in protein levels are dampened, protein levels are mostly driven toward peak rather than nadir levels.

Many possibilities exist for the upstream signaling that drives the sleep- and circadian-dependent accumulation of RNA and proteins that we observed. Whereas the mechanism connecting cellular components of the circadian oscillator to downstream pathways is well established (*62*, *63*), neither the workings of the sleep homeostat itself nor its connection to downstream sleep-dependent cellular events has been deciphered. In addition to the direct synaptic activity–dependent hypotheses that we favor (*20*), indirect mechanisms such as changes in brain temperature and cortisol levels are also possible. Changes in transcript abundance associated with small alterations in body temperature are believed to be mediated either by an initial posttranscriptional effect by the cold-inducible RNA-binding protein CIRBP (*64*) or by low-level activation of Heat Shock Factor 1 (*65*). We have found no overlap between mRNAs regulated by these factors and our cycling dataset, making it unlikely that temperature changes are responsible for the effects that we observed. Similarly, although cortisol elevations during wake and especially during sleep deprivation are well documented, adrenalectomy experiments establish that cortisol is not responsible for most of the transcriptional effects of SD (*66*). Therefore, we also disfavor this indirect cue as a primary signal.

Overall, our results are consistent with anticipatory circadian delivery of synaptic mRNAs before dawn and dusk, followed by "need-dependent" local translation linked to sleep and wake states. These spatiotemporal dynamics across the synaptic landscape likely play

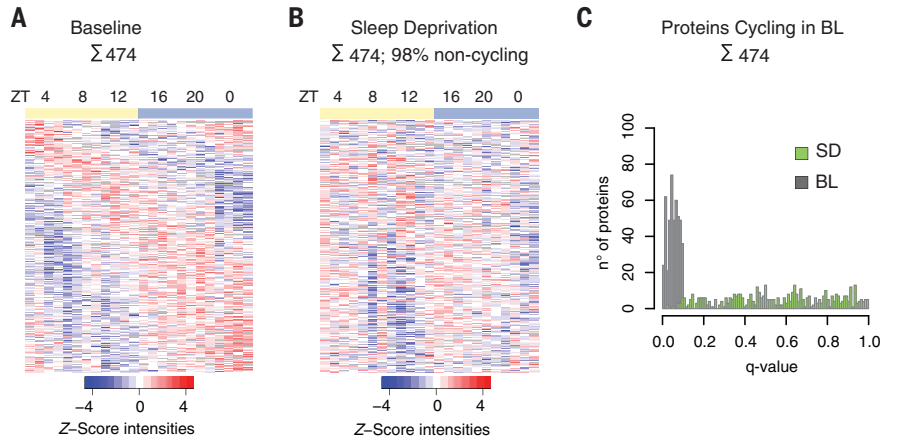

Fig. 8. The synaptic proteome shows oscillations almost entirely dependent upon sleep-wake state. (**A** and **B**) Heatmap of label free intensities of cycling proteins in BL (A) and the corresponding values in SD (B) in all biological replicates for each sampled time point (columns). Proteins (in rows) are ordered by the estimated phase in BL, and all intensities in both conditions were *z*-scored to BL intensity values. (Note: of the 474 proteins represented, 98% did not cycle in SD.) (**C**) Distribution of the *q* values (Perseus time-series periodic analysis, period 24 hours) of the cycling synaptic proteome in BL (gray) and the corresponding *q* value in the SD dataset (green).

a critical role in diurnally regulating all aspects of forebrain function.

Materials and Methods

Animals and tissue collection

All experiments were performed after approval by the animal welfare officer of the University of Zürich and veterinary authorities of the Canton of Zürich. Ten-week-old male C57BL/6 mice were housed with free access to food and water and entrained to a 12 hour:12 hour LD schedule for 14 days. Mice were sacrificed at 4-hour intervals over 1 day (ZT0, ZT4, ZT8, ZT12, ZT16, and ZT20; n = 3 mice for transcriptome and n = 4 mice for proteome). At the time points overlapping with light transitions (ZT0 and ZT12), euthanasia was performed right before the light change. For the around-the-clock sleep deprivation, mice were allowed to acclimatize to a 12-hour light/12-hour dark cycle for 14 days. Six groups of mice were sleep deprived for 4 hours by gentle handling [cage exchange and introduction of new objects as described previously (*67*)] at different times of day [SD4 (sleep deprivation from ZT0 to ZT4), SD8, SD12, SD16, SD20, and SD0; n = 3 mice for transcriptome and n = 4 mice for proteome]. To collect synaptoneurosomes from mice kept in constant darkness and from *Bmal1*$^{-/-}$ mice, animals were kept in LD for 2 weeks and then transferred to constant darkness (DD) 48 hours before euthanasia at circadian times (CT) CT0 and CT12, respectively (n = 3).

EEG recording and sleep data analysis

Adult C57BL/6 mice were used for surgery (8 to 10 weeks old at surgery). Mice were implanted epidurally under isoflurane anesthesia for EEG recording. Right before and 24 hours after surgery, mice were treated with an analgesic (Temgesic, 0.1 mg/kg, intraperitoneal). Gold-plated miniature screws (0.9-mm diameter) were used as EEG electrodes and positioned on the left hemisphere above the frontal cortex (1.5 mm anterior to bregma, 1.5 mm lateral to the midline) and the parietal cortex (2 mm posterior to bregma, 2 mm lateral to the midline). The reference electrode was placed above the cerebellum (2 mm posterior to lambda, 0 mm lateral to the midline). Screws were connected to copper wires and fixed to the skull with dental cement (Paladur two-component system). Electromyography (EMG) was recorded using two gold wires (0.2-mm diameter) inserted bilaterally in the neck muscle. After 1 week of recovery, EEG and EMG were recorded continuously for 7 days. Two cohorts of six and eight mice, respectively, underwent 1 day of BL recording and 3 days of SD recording, with 48 hours of recovery in between. Cohort 1 underwent SD at ZT4 to ZT8, ZT12 to ZT16, and ZT16 to ZT20. Cohort 2 underwent SD at ZT0 to ZT4, ZT8 to ZT12, and ZT20 to ZT24. SD was performed by gentle handling as described previously (*67*). Both EEG and EMG signals were amplified (factor 2000), analog filtered (high-pass filter: −3 dB at 0.016 Hz; low-pass filter: −3 dB at 40 Hz, <−35 dB at 128 Hz), sampled with 512 Hz, digitally filtered (EEG, low-pass FIR filter: 25 Hz; EMG, band-pass FIR filter: 20 to 50 Hz), and stored with a 128-Hz resolution. EEG power spectra were computed for 4-s epochs by a fast Fourier transform routine within the frequency range of 0.5 to 25 Hz. Between 0.5 and 5 Hz, 0.5-Hz bins were used, and between 5 and 25 Hz, 1-Hz bins were used. The corresponding slow-wave-activity (SWA) was calculated using the raw parietal and frontal EEG, as well as the raw and integrated EMG, to visually score three vigilance states: non-rapid eye movement (NREM) sleep, rapid eye movement sleep (REM), and wake, for 4-s epochs. Epochs containing artifacts were identified and excluded from the spectral analysis. Data analysis was carried out using MATLAB version R2015a (The MathWorks, Inc., Natick, MA, USA). Relative frontal SWA was calculated relative to the mean SWA at ZT8 to ZT12 during the BL day. Sleep loss was calculated by comparing NREM sleep amount in each 4-h SD slot with the sleep amount in the same time of day of the corresponding BL day [$p < 0.05$, one-way analysis of variance (ANOVA)]. Sleep latency was analyzed by measuring the time each mouse stayed awake after the end of each 4-h SD until it slept for >1 min ($p < 0.05$, one-way ANOVA).

Purification of synaptoneurosomes

Synaptoneurosomes from mouse forebrain were prepared as described previously (*22*). In brief, brain was isolated and rapidly cooled to 4°C, washed in ice-cooled sucrose buffer (320 mM sucrose, 5 mM HEPES, pH 7.4), followed by homogenization with a Teflon-glass tissue grinder using a motor-driven pestle keeping samples cooled. Homogenate was centrifuged at 1000*g* for 10 min. Two milliliters of the supernatant was loaded over discontinuous Percoll gradients (3, 10, and 23% Percoll in sucrose buffer) and centrifuged at 31,000*g* for 5 min. The fractions at the interfaces between 3 and 10% and 10 and 23% were collected and further centrifuged at 20,000*g* to pellet synaptoneurosomes. All centrifugation steps were performed at 4°C. All solutions were supplemented with complete protease inhibitor cocktail (Roche), 0.05 mM dithiothreitol (DTT), 0.1 mM phenylmethylsulfonyl fluoride, and 20 U/10 μl RNaseOUT (Invitrogen).

RNA sample preparation

Two hundred microliters of homogenate was used for total RNA extraction. Briefly, tissue lysate in QIAzol Lysis Reagent (Qiagen) was vortexed for few seconds. Then, 0.2 ml of chloroform was added to lysate and mixed by vigorous shaking for 15 s. The mixture was incubated at room temperature for 10 min and centrifuged at 18,000*g* for 20 min at 4°C to separate phases. The upper aqueous phase containing RNA was carefully aspirated to a fresh, nuclease-free tube. The RNA was then precipitated by adding one volume of isopropanol and centrifuged at 18,000*g* for 20 min at 4°C. The RNA pellet was washed with 70% ethanol, air-dried, and dissolved in nuclease-free water.

Frozen synaptoneurosome pellets (~500 μl) were processed with the High Pure RNA Isolation Kit (Roche). Samples were mixed with 600 μl of lysis binding buffer and further steps were performed according to the manufacturer's instructions. The dissolved total RNA was

quantified by NanoDrop (NanoDrop Technologies) and a Qubit (1.0) Fluorometer (Life Technologies, Pleasanton, CA, USA). The quality was assessed with a 2100 Bioanalyzer (Agilent Technologies, Waldbronn, Germany).

Library preparation, sequencing, and data processing

Poly(A) RNA sequencing was performed using 500 μg of total RNA. Strand-specific cDNA libraries were prepared using Illumina's TruSeq Stranded Sample Prep Kit (125-bp single-read mode) following the manufacturer's directions, then sequenced on a HiSeq 4000 (Illumina Inc., San Diego, CA, USA). The raw reads were first cleaned by removing adapter sequences, trimming low-quality ends, and filtering reads with low quality (phred quality <20) using Trimmomatic (versions 0.33 and 0.36) (*68*). Specific quality control measures were evaluated and the following samples were excluded: replicate number 3 in ZT16 BL because of degradation during the library preparation; one sample from ZT8 BL because of reduced read counts (<10 million); and two samples from ZT4 SD, three from ZT16 SD, and three from ZT20 SD because of signs of contamination with external material. Sequence alignment of the resulting high-quality reads to the mouse reference genome (build GRCm38) and quantification of gene-level expression was performed using RSEM (versions 1.2.22 and 1.3.0) (*69*). For downstream analysis, the mRNA features were filtered according to normalized (log mean) feature counts, which represent aggregated raw counts of mapped reads at the gene level (RSEM). We determined a threshold for minimum gene expression on the basis of the assumption that a transcript with >10 counts in two of three replicates is expressed (linear signal threshold of 10).

Bioinformatic and statistical analyses of transcriptomics data

To search for transcripts that are enriched in neuronal synapses, we did a differential gene expression analysis using a pairwise comparison between synaptoneurosomes and whole brain at two time points, ZT0 and ZT12. The threshold to consider a gene enriched in the synapse was a fold change (of the synaptic samples versus the whole forebrain samples) >1.5 in one of the two time points.

Cycling analysis was performed using the computational platform Perseus (*25*). We fit the normalized mRNA counts to a cosine with a fixed period of 24 hours and with amplitude and phase as free parameters (*9*). Profiles were ranked by their variance ratio. This was the part of the variance explained by the fit divided by the contribution to the variance that was not accounted for by the fit. On the basis of this ranking, we determined a permutation-based false discovery rate (FDR) by repeating the same procedure 1000 times on the same profiles but with randomized time labels. We used a statistical cutoff of $q < 0.05$ to define the cycling transcriptome. Hierarchical clustering was performed in a phase-preserving manner by restricting the order of elements to that determined by the output of the cosine model-based fitting. Amplitudes were calculated as the $\log_2$ of the fold change of counts. To evaluate the effect of constant darkness and the lack of a functional clock on the generation of the peaks of synaptic transcript accumulation, we compared the following conditions: ZT0 versus CT0, ZT0 versus CT0 *Bmal*$^{-/-}$, ZT12 versus CT12, and ZT12 versus CT12 *Bmal1*$^{-/-}$, by applying a count-based negative binomial model implemented in the software package EdgeR (R version: 3.4.2, EdgeR version: 3.20.1) (*70*). The differential expression was assessed using an exact test adapted for overdispersed data. Genes showing altered expression with an adjusted (BH method) $p < 0.05$ were considered differentially expressed.

Protein sample preparation

For protein extraction, 4% SDS was added to each synaptoneurosomal sample or to the homogenate, followed by 5 min of incubation at 95°C. Samples were flash frozen and stored at −80°C until used. Samples were lysed (0.1 mM Tris-HCl, pH 7.6, and 4% SDS), sonicated in a Bioruptor (Diagenode) at 4°C for 15 min or until homogeneous suspension was formed, and boiled at 95°C for 5 min. Protein lysates were treated first with 1 μl of DTT (1 M), followed by 10 μl 2-chloroacetamide (0.5 M). Each treatment was performed at room temperature (22°C) for 20 min. The lysates were precipitated with acetone as described previously (*9*). In detail, pellets were resuspended in 500 μl of trifluoroethanol digestion buffer. For protein digestion 1:100 (protein:enzyme) trypsin and LysC were added and samples incubated overnight at 37°C with rapid agitation (1500 rpm). Digested peptides were concentrated in a SpeedVac for 15 min at 45°C, followed by acidification using 10 μl of 10% trifluoroacetic acid (TFA). Peptides were then desalted using StageTips with two layers of styrenedivinylbenzene–reversed phase sulfonated (SDB-RPS; 3M Empore), washed twice with wash buffer (0.2% TFA), and then washed once with isopropanol containing 1% TFA. Peptides were eluted by adding 60 μl of SDB-RPS elution buffer [80% acetonitrile, 1.25% NH_4OH (25% high-performance liquid chromatography grade)] and immediately concentrated in a SpeedVac for 30 min at 45°C. Concentrated peptides were then resuspended in a buffer containing 2% ACN and 0.1% TFA before chromatography–tandem mass spectrometry (LC-MS/MS) analysis.

LC-MS/MS analysis and data processing

Samples were measured in a single shot (*71*), loading ~2 μg of peptide mixture onto a 50-cm reversed-phase column (diameter 75 μM; packed in-house with 1.9 μM C18 ReproSil particles; Dr. Maisch GmbH). The temperature of the homemade column oven was maintained at 60°C. The column was mounted to the EASY-nLC 1200 system (Thermo Fisher Scientific). The peptides were eluted with a binary buffer system consisting of buffer A (0.1% formic acid) and buffer B (80% ACN and 0.1% formic acid). A gradient length of 140 min was chosen (5 to 65% buffer B for 130 min followed by 10 min of 80% buffer B) with a flow rate of 300 nl/min. Peptides were then electrosprayed into a Q Exactive HF mass spectrometer (MS) (Thermo Fisher Scientific), obtaining full scans (300 to 1650 m/z, R = 60,000 at 200 m/z) at a target of 3×10^6 ions. The 15 most abundant ions were selected and fragmented with higher-energy collisional dissociation (target 1×10^5 ions, maximum injection time 60 ms, isolation window 1.4 m/z, underfill ratio 1%), followed by detection in the Orbitrap (R = 15,000 at 200 m/z). Raw MS data files were processed using MaxQuant [version 1.5.5.6 (24)] to calculate label free intensities with the Andromeda search engine with FDR < 0.01 at the protein and peptide levels. The default settings were used with the following modifications: (i) the variable modification methionine (M), acetylation (protein N terminus), and the fixed modification carbamidomethyl (C) were selected; (ii) only peptides with a minimal length of seven amino acids were considered; and (iii) the "match between run" option was enabled with a matching time window of 0.7 min. For protein and peptide identification, the UniProt database from mouse (September 2014) including 51,210 entries was used. Each raw file and replicate was treated as one independent experiment.

Bioinformatic and statistical analyses of proteomics data

Processed data were uploaded in Perseus software (*25*). First, reverse sequences and potential contaminants were removed. Then, the total dataset was $\log_2$ transformed and label free intensities were normalized in each sample by subtracting the media of all intensities in the same sample. Proteins without label free intensities in <10 samples were removed in both the synaptoneurosomes (SD/BL) and total forebrain datasets. Replicates 1 and 4 of ZT4, replicate 4 of ZT8, and replicate 1 of ZT12 of the total brain homogenate were not considered because the protein quantification in these samples was limited.

Cycling analysis was done as for the transcriptomic data, in this case using protein intensity values. Amplitudes were as well calculated as the $\log_2$-fold change. For comparison of transcriptome and the proteome data, we matched datasets by gene name or Uniprot ID.

GO analysis

All ontological analyses were done with the enrichment analysis tool FunRich using the Hgcn gene symbols. For analysis of synaptic enriched mRNAs (3104, of which 2954 were available in the database), the GO option "GOTERM Cellular Component" was selected. A maximum p value of 0.001 was chosen to select only significant categories. For the evaluation of synaptic enrichment, we filtered for annotations containing the following terms: "synap*," "project*," "dendr*," "axon," or "spine." The percentage of genes for each annotation and the fold enrichment in the three categories, identified, expressed, and enriched features, were used to validate the enrichment strategy. Only the top 10 annotations according to p value were included in the graphical representation; all returned annotations are shown in the supplementary tables. Enriched biological processes of the cycling transcriptome were identified separately for light (752, of which 725 were available in the "Biological Process" database feature in GO) or dark phases (1263, of which 1217 were available in the Biological Process database). Features were ascribed to each group using hierarchical clustering according to the temporal expression profile. Annotation with a BH-corrected $p < 0.001$ was included. Enrichment for biological processes in the synaptic enriched dataset was also performed for comparison of the common annotations. To compare the annotation enrichment between the light and dark clusters, we performed a fold enrichment analysis between both datasets and obtained a fold value (included in table S4). To analyze the gene datasets obtained after the SD experiment. we followed similar steps. Four groups of features were independently analyzed according to phase or cycling behavior in SD (light and $q < 0.05$, 149 features; light and $q > 0.05$, 603 features; dark and $q < 0.05$, 393 features; dark and $q > 0.05$, 863 features). For representation, the top 10 enriched annotations (ranked by the fold value between phases for cycling or not in SD and vice versa and with BH-corrected $p < 0.1$) were considered. For the common cycling features at the mRNA and transcript levels, the phase of protein was used to classify each into the light cluster (29 features) or dark cluster (27 features). For representation, we selected the top five enriched annotations (BH-corrected $p < 0.01$).

Single-molecule RNA in situ hybridization

RNAscope hybridization was performed with the RNAscope Multiplex Fluorescent v2-kit (Advanced Cell Diagnostics, Inc.) according to the manufacturer's instructions with the following modifications. Mice were perfused intracardially with artificial cerebral spinal fluid, the dissected brains postfixed with 4% paraformaldehyde for 2 hours at 4°C, and subsequently cryoprotected in 30% sucrose in PBS for 24 hours at 4°C and frozen at −80°C for up to 3 months. The brains were cut coronally at 14 μm with a cryotome, mounted on a SuperFrost glass slide (Thermo Fisher Scientific), and stored at −80°C until use. Tissue sections were then dried in the ACD hybridizer at 37°C for at least 1 hour, treated with hydrogen peroxide for 10 min, and dried before protease treatment at 60°C for 30 min. The boiling step in the antigen-retrieval procedure has been omitted and the sections were digested in Protease Plus (Advanced Cell Diagnostics, Inc.) solution for 15 min at 40°C. Each RNA signal has been developed sequentially by specifically targeting each probe with horseradish peroxidase, which converted fluorescently labeled tyramide (TSA Plus fluorescein, Cy3 or Cy5 kit, PerkinElmer) into an insoluble stain around the RNA of interest. The final concentration of tyramide in TSA buffer solution was 1:1500. Custom RNAscope target probes (all targeting mouse transcripts) were purchased from Advanced Cell Diagnostics (*Slc17a7*, *Lingo1*, and *Cry1*), as well as standard RNAscope positive (housekeeping genes: *PolR2a*, *PPIB* and *Ubc*) and negative (bacterial housekeeping gene: *DapB*) control probes.

For imaging, a confocal laser-scanning microscope (LSM 710, Carl Zeiss, ZEN imaging software) was used. The images were acquired using a 40× (numerical aperture 1.4) objective and a pinhole set at 1 airy unit, pixel dwell time 3.15 μs, and laser power 1.2 to 2%. The images spanned the whole thickness of the brain slices (10 to 12 μm) in 1-μm steps and were analyzed as a maximum-intensity projection across z-stacks.

To reliably quantify mRNA dots in different brain regions, a custom Python script was written using the ImageJ image-processing framework. The script can be used as a plugin and is openly available on a GitHub repository (https://github.com/dcolam/Cluster-Analysis-Plugin). Images were binarized and segmented to separate nuclei-rich regions (pyramidal cell layer of the hippocampus and cell nuclei in cortex), and particle analysis was done using ImageJ. For representation purposes, mRNA dots were enlarged to improve visualization.

REFERENCES AND NOTES

1. K. F. Storch *et al*., Intrinsic circadian clock of the mammalian retina: Importance for retinal processing of visual information. *Cell* **130**, 730–741 (2007). doi: 10.1016/j.cell.2007.06.045; pmid: 17719549
2. R. Zhang, N. F. Lahens, H. I. Ballance, M. E. Hughes, J. B. Hogenesch, A circadian gene expression atlas in mammals: Implications for biology and medicine. *Proc. Natl. Acad. Sci. U.S.A.* **111**, 16219–16224 (2014). doi: 10.1073/pnas.1408886111; pmid: 25349387
3. S. Maret *et al*., Homer1a is a core brain molecular correlate of sleep loss. *Proc. Natl. Acad. Sci. U.S.A.* **104**, 20090–20095 (2007). doi: 10.1073/pnas.0710131104; pmid: 18077435
4. S. Panda *et al*., Coordinated transcription of key pathways in the mouse by the circadian clock. *Cell* **109**, 307–320 (2002). doi: 10.1016/S0092-8674(02)00722-5; pmid: 12015981
5. N. Koike *et al*., Transcriptional architecture and chromatin landscape of the core circadian clock in mammals. *Science* **338**, 349–354 (2012). doi: 10.1126/science.1226339; pmid: 22936566
6. D. Feng *et al*., A circadian rhythm orchestrated by histone deacetylase 3 controls hepatic lipid metabolism. *Science* **331**, 1315–1319 (2011). doi: 10.1126/science.1198125; pmid: 21393543
7. I. Schmutz, J. A. Ripperger, S. Baeriswyl-Aebischer, U. Albrecht, The mammalian clock component PERIOD2 coordinates circadian output by interaction with nuclear receptors. *Genes Dev.* **24**, 345–357 (2010). doi: 10.1101/gad.564110; pmid: 20159955
8. G. Rey *et al*., Genome-wide and phase-specific DNA-binding rhythms of BMAL1 control circadian output functions in mouse liver. *PLOS Biol.* **9**, e1000595 (2011). doi: 10.1371/journal.pbio.1000595; pmid: 21364973
9. M. S. Robles, J. Cox, M. Mann, In-vivo quantitative proteomics reveals a key contribution of post-transcriptional mechanisms to the circadian regulation of liver metabolism. *PLOS Genet.* **10**, e1004047 (2014). doi: 10.1371/journal.pgen.1004047; pmid: 24391516
10. B. G. Robinson, D. M. Frim, W. J. Schwartz, J. A. Majzoub, Vasopressin mRNA in the suprachiasmatic nuclei: Daily regulation of polyadenylate tail length. *Science* **241**, 342–344 (1988). doi: 10.1126/science.3388044; pmid: 3388044
11. V. Bélanger, N. Picard, N. Cermakian, The circadian regulation of Presenilin-2 gene expression. *Chronobiol. Int.* **23**, 747–766 (2006). doi: 10.1080/07420520600827087; pmid: 16887746
12. C. Vollmers *et al*., Time of feeding and the intrinsic circadian clock drive rhythms in hepatic gene expression. *Proc. Natl. Acad. Sci. U.S.A.* **106**, 21453–21458 (2009). doi: 10.1073/pnas.0909591106; pmid: 19940241
13. K. S. Kosik, Life at Low Copy Number: How Dendrites Manage with So Few mRNAs. *Neuron* **92**, 1168–1180 (2016). doi: 10.1016/j.neuron.2016.11.002; pmid: 28009273
14. A. R. Buxbaum, G. Haimovich, R. H. Singer, In the right place at the right time: Visualizing and understanding mRNA localization. *Nat. Rev. Mol. Cell Biol.* **16**, 95–109 (2015). doi: 10.1038/nrm3918; pmid: 25549890
15. J. L. Dynes, O. Steward, Dynamics of bidirectional transport of Arc mRNA in neuronal dendrites. *J. Comp. Neurol.* **500**, 433–447 (2007). doi: 10.1002/cne.21189; pmid: 17120280
16. R. B. Knowles *et al*., Translocation of RNA granules in living neurons. *J. Neurosci.* **16**, 7812–7820 (1996). doi: 10.1523/JNEUROSCI.16-24-07812.1996; pmid: 8987809
17. S. Miller *et al*., Disruption of dendritic translation of CaMKIIalpha impairs stabilization of synaptic plasticity and memory consolidation. *Neuron* **36**, 507–519 (2002). doi: 10.1016/S0896-6273(02)00978-9; pmid: 12408852
18. S. Hutten, T. Sharangdhar, M. Kiebler, Unmasking the messenger. *RNA Biol.* **11**, 992–997 (2014). doi: 10.4161/rna.32091; pmid: 25482894
19. G. H. Diering *et al*., Homer1a drives homeostatic scaling-down of excitatory synapses during sleep. *Science* **355**, 511–515 (2017). doi: 10.1126/science.aai8355; pmid: 28154077
20. G. Tononi, C. Cirelli, Sleep and the price of plasticity: From synaptic and cellular homeostasis to memory consolidation and integration. *Neuron* **81**, 12–34 (2014). doi: 10.1016/j.neuron.2013.12.025; pmid: 24411729
21. S. Ray, A. B. Reddy, Cross-talk between circadian clocks, sleep-wake cycles, and metabolic networks: Dispelling the darkness. *BioEssays* **38**, 394–405 (2016). doi: 10.1002/bies.201500056; pmid: 26866932
22. P. R. Dunkley, P. E. Jarvie, P. J. Robinson, A rapid Percoll gradient procedure for preparation of synaptosomes. *Nat. Protoc.* **3**, 1718–1728 (2008). doi: 10.1038/nprot.2008.171; pmid: 18927557
23. I. J. Cajigas *et al*., The local transcriptome in the synaptic neuropil revealed by deep sequencing and high-resolution imaging. *Neuron* **74**, 453–466 (2012). doi: 10.1016/j.neuron.2012.02.036; pmid: 22578497
24. R. Ouwenga *et al*., Transcriptomic Analysis of Ribosome-Bound mRNA in Cortical Neurites *In Vivo*. *J. Neurosci.* **37**, 8688–8705 (2017). doi: 10.1523/JNEUROSCI.3044-16.2017; pmid: 28821669
25. S. Tyanova *et al*., The Perseus computational platform for comprehensive analysis of (prote)omics data. *Nat. Methods* **13**, 731–740 (2016). doi: 10.1038/nmeth.3901; pmid: 27348712
26. M. E. Hughes, J. B. Hogenesch, K. Kornacker, JTK_CYCLE: An efficient nonparametric algorithm for detecting rhythmic components in genome-scale data sets. *J. Biol. Rhythms* **25**, 372–380 (2010). doi: 10.1177/0748730410379711; pmid: 20876817
27. R. T. Fremeau Jr., S. Voglmaier, R. P. Seal, R. H. Edwards, VGLUTs define subsets of excitatory neurons and suggest novel roles for glutamate. *Trends Neurosci.* **27**, 98–103 (2004). doi: 10.1016/j.tins.2003.11.005; pmid: 15102489

28. A. Karlén *et al*., Nogo receptor 1 regulates formation of lasting memories. *Proc. Natl. Acad. Sci. U.S.A.* **106**, 20476–20481 (2009). doi: 10.1073/pnas.0905390106; pmid: 19915139
29. A. Jilg *et al*., Temporal dynamics of mouse hippocampal clock gene expression support memory processing. *Hippocampus* **20**, 377–388 (2010). pmid: 19437502
30. M. Megías, Z. Emri, T. F. Freund, A. I. Gulyás, Total number and distribution of inhibitory and excitatory synapses on hippocampal CA1 pyramidal cells. *Neuroscience* **102**, 527–540 (2001). doi: 10.1016/S0306-4522(00)00496-6; pmid: 11226691
31. M. K. Bunger *et al*., Mop3 is an essential component of the master circadian pacemaker in mammals. *Cell* **103**, 1009–1017 (2000). doi: 10.1016/S0092-8674(00)00205-1; pmid: 11163178
32. P. Franken, D. Chollet, M. Tafti, The homeostatic regulation of sleep need is under genetic control. *J. Neurosci.* **21**, 2610–2621 (2001). doi: 10.1523/JNEUROSCI.21-08-02610.2001; pmid: 11306614
33. D. Bell-Pedersen *et al*., Circadian rhythms from multiple oscillators: Lessons from diverse organisms. *Nat. Rev. Genet.* **6**, 544–556 (2005). doi: 10.1038/nrg1633; pmid: 15951747
34. H. Nakatsuka, K. Natsume, Circadian rhythm modulates long-term potentiation induced at CA1 in rat hippocampal slices. *Neurosci. Res.* **80**, 1–9 (2014). doi: 10.1016/j.neures.2013.12.007; pmid: 24406747
35. T. A. Wang *et al*., Circadian rhythm of redox state regulates excitability in suprachiasmatic nucleus neurons. *Science* **337**, 839–842 (2012). doi: 10.1126/science.1222826; pmid: 22859819
36. C. M. Pennartz, R. Hamstra, A. M. Geurtsen, Enhanced NMDA receptor activity in retinal inputs to the rat suprachiasmatic nucleus during the subjective night. *J. Physiol.* **532**, 181–194 (2001). doi: 10.1111/j.1469-7793.2001.0181g.x; pmid: 11283234
37. K. Richter *et al*., VGLUT1 Binding to Endophilin or Intersectin1 and Dynamin Phosphorylation in a Diurnal Context. *Neuroscience* **371**, 29–37 (2018). doi: 10.1016/j.neuroscience.2017.11.034; pmid: 29199069
38. G. Benegiamo, S. A. Brown, S. Panda, RNA Dynamics in the Control of Circadian Rhythm. *Adv. Exp. Med. Biol.* **907**, 107–122 (2016). doi: 10.1007/978-3-319-29073-7_5; pmid: 27256384
39. S. Kojima, M. Hirose, K. Tokunaga, Y. Sakaki, H. Tei, Structural and functional analysis of 3′ untranslated region of mouse Period1 mRNA. *Biochem. Biophys. Res. Commun.* **301**, 1–7 (2003). doi: 10.1016/S0006-291X(02)02938-8; pmid: 12535631
40. E. Y. Kim *et al*., Drosophila CLOCK protein is under posttranscriptional control and influences light-induced activity. *Neuron* **34**, 69–81 (2002). doi: 10.1016/S0896-6273(02)00639-6; pmid: 11931742
41. B. L. Timney *et al*., Simple kinetic relationships and nonspecific competition govern nuclear import rates in vivo. *J. Cell Biol.* **175**, 579–593 (2006). doi: 10.1083/jcb.200608141; pmid: 17116750
42. T. Dange, D. Grünwald, A. Grünwald, R. Peters, U. Kubitscheck, Autonomy and robustness of translocation through the nuclear pore complex: A single-molecule study. *J. Cell Biol.* **183**, 77–86 (2008). doi: 10.1083/jcb.200806173; pmid: 18824568
43. A. Zappulo *et al*., RNA localization is a key determinant of neurite-enriched proteome. *Nat. Commun.* **8**, 583 (2017). doi: 10.1038/s41467-017-00690-6; pmid: 28928394
44. O. Rawashdeh *et al*., PERIOD1 coordinates hippocampal rhythms and memory processing with daytime. *Hippocampus* **24**, 712–723 (2014). doi: 10.1002/hipo.22262; pmid: 24550127
45. W. Hauber, A. Bareiss, Facilitative effects of an adenosine A1/A2 receptor blockade on spatial memory performance of rats: Selective enhancement of reference memory retention during the light period. *Behav. Brain Res.* **118**, 43–52 (2001). doi: 10.1016/S0166-4328(00)00307-7; pmid: 11163632
46. Y. Takahashi, K. Sawa, T. Okada, The diurnal variation of performance of the novel location recognition task in male rats. *Behav. Brain Res.* **256**, 488–493 (2013). doi: 10.1016/j.bbr.2013.08.040; pmid: 24008072
47. K. L. Eckel-Mahan *et al*., Circadian oscillation of hippocampal MAPK activity and cAmp: Implications for memory persistence. *Nat. Neurosci.* **11**, 1074–1082 (2008). doi: 10.1038/nn.2174; pmid: 19160506
48. J. J. Zhu, Y. Qin, M. Zhao, L. Van Aelst, R. Malinow, Ras and Rap control AMPA receptor trafficking during synaptic plasticity. *Cell* **110**, 443–455 (2002). doi: 10.1016/S0092-8674(02)00897-8; pmid: 12202034
49. P. Chen, Z. Gu, W. Liu, Z. Yan, Glycogen synthase kinase 3 regulates N-methyl-D-aspartate receptor channel trafficking and function in cortical neurons. *Mol. Pharmacol.* **72**, 40–51 (2007). doi: 10.1124/mol.107.034942; pmid: 17400762
50. M. Ikeda *et al*., Hippocampal spine changes across the sleep-wake cycle: Corticosterone and kinases. *J. Endocrinol.* **226**, M13–M27 (2015). doi: 10.1530/JOE-15-0078; pmid: 26034071
51. J. H. Benington, H. C. Heller, Restoration of brain energy metabolism as the function of sleep. *Prog. Neurobiol.* **45**, 347–360 (1995). doi: 10.1016/0301-0082(94)00057-O; pmid: 7624482
52. M. Mackiewicz *et al*., Macromolecule biosynthesis: A key function of sleep. *Physiol. Genomics* **31**, 441–457 (2007). doi: 10.1152/physiolgenomics.00275.2006; pmid: 17698924
53. F. Brüning *et al*., Sleep-wake cycles drive daily dynamics of synaptic phosphorylation. *Science* **366**, XXX–XXX (2019).
54. A. Laposky *et al*., Deletion of the mammalian circadian clock gene BMAL1/Mop3 alters baseline sleep architecture and the response to sleep deprivation. *Sleep* **28**, 395–409 (2005). doi: 10.1093/sleep/28.4.395; pmid: 16171284
55. J. P. Wisor *et al*., A role for cryptochromes in sleep regulation. *BMC Neurosci.* **3**, 20 (2002). doi: 10.1186/1471-2202-3-20; pmid: 12495442
56. L. de Vivo *et al*., Ultrastructural evidence for synaptic scaling across the wake/sleep cycle. *Science* **355**, 507–510 (2017). doi: 10.1126/science.aah5982; pmid: 28154076
57. M. Jasinska *et al*., Circadian rhythmicity of synapses in mouse somatosensory cortex. *Eur. J. Neurosci.* **42**, 2585–2594 (2015). doi: 10.1111/ejn.13045; pmid: 26274013
58. J. A. Ainsley, L. Drane, J. Jacobs, K. A. Kittelberger, L. G. Reijmers, Functionally diverse dendritic mRNAs rapidly associate with ribosomes following a novel experience. *Nat. Commun.* **5**, 4510 (2014). doi: 10.1038/ncomms5510; pmid: 25072471
59. S. Hüttelmaier *et al*., Spatial regulation of beta-actin translation by Src-dependent phosphorylation of ZBP1. *Nature* **438**, 512–515 (2005). doi: 10.1038/nature04115; pmid: 16306994
60. K. M. Huber, M. S. Kayser, M. F. Bear, Role for rapid dendritic protein synthesis in hippocampal mGluR-dependent long-term depression. *Science* **288**, 1254–1257 (2000). doi: 10.1126/science.288.5469.1254; pmid: 10818003
61. K. C. Martin *et al*., Synapse-specific, long-term facilitation of aplysia sensory to motor synapses: A function for local protein synthesis in memory storage. *Cell* **91**, 927–938 (1997). doi: 10.1016/S0092-8674(00)80484-5; pmid: 9428516
62. S. A. Brown, A. Azzi, Peripheral circadian oscillators in mammals. *Handb. Exp. Pharmacol.* **217**, 45–66 (2013). doi: 10.1007/978-3-642-25950-0_3; pmid: 23604475
63. M. Brancaccio *et al*., Network-mediated encoding of circadian time: The suprachiasmatic nucleus (SCN) from genes to neurons to circuits, and back. *J. Neurosci.* **34**, 15192–15199 (2014). doi: 10.1523/JNEUROSCI.3233-14.2014; pmid: 25392488
64. J. Morf *et al*., Cold-inducible RNA-binding protein modulates circadian gene expression posttranscriptionally. *Science* **338**, 379–383 (2012). doi: 10.1126/science.1217726; pmid: 22923437
65. A. Neueder *et al*., HSF1-dependent and -independent regulation of the mammalian in vivo heat shock response and its impairment in Huntington's disease mouse models. *Sci. Rep.* **7**, 12556 (2017). doi: 10.1038/s41598-017-12897-0; pmid: 28970536
66. V. Mongrain *et al*., Separating the contribution of glucocorticoids and wakefulness to the molecular and electrophysiological correlates of sleep homeostasis. *Sleep* **33**, 1147–1157 (2010). doi: 10.1093/sleep/33.9.1147; pmid: 20857860
67. I. Tobler, K. Jaggi, Sleep and EEG spectra in the Syrian hamster (*Mesocricetus auratus*) under baseline conditions and following sleep deprivation. *J. Comp. Physiol. A* **161**, 449–459 (1987). doi: 10.1007/BF00603970; pmid: 3668881
68. A. M. Bolger, M. Lohse, B. Usadel, Trimmomatic: A flexible trimmer for Illumina sequence data. *Bioinformatics* **30**, 2114–2120 (2014). doi: 10.1093/bioinformatics/btu170; pmid: 24695404
69. B. Li, C. N. Dewey, RSEM: Accurate transcript quantification from RNA-Seq data with or without a reference genome. *BMC Bioinformatics* **12**, 323 (2011). doi: 10.1186/1471-2105-12-323; pmid: 21816040
70. M. D. Robinson, D. J. McCarthy, G. K. Smyth, edgeR: A Bioconductor package for differential expression analysis of digital gene expression data. *Bioinformatics* **26**, 139–140 (2010). doi: 10.1093/bioinformatics/btp616; pmid: 19910308
71. N. Nagaraj *et al*., System-wide perturbation analysis with nearly complete coverage of the yeast proteome by single-shot ultra HPLC runs on a bench top Orbitrap. *Mol. Cell. Proteomics* **11**, 013722 (2012). doi: 10.1074/mcp.M111.013722; pmid: 22021278
72. S. B. Noya *et al*., mRNA in situ images for: The forebrain synaptic transcriptome is organized by clocks but its proteome is driven by sleep, Zenodo (2019); https://doi.org/10.5281/zenodo.2546770

ACKNOWLEDGMENTS

We are grateful to the Functional Genomics Center Zürich (FGCZ) for transcriptomics services, and to Juergen Cox and the Max Planck Institute of Biochemistry, Münich, for proteomics services. **Funding:** S.A.B. and S.B.N. were supported by the Swiss National Science Foundation, the Velux Foundation, the Human Frontiers Science Program, and the Zürich Clinical Research Priority Project "Sleep and Health." S.B.N. and S.K.T. were further supported by a Ph.D. grant from the Zürich Neurozentrum. All three are members of the Neurosciences Program within the Life Sciences Zürich Graduate School. M.S.R., F.B., and M.M. were supported by the Max-Planck Society for the Advancement of Sciences and the German Research Foundation (DFG/Gottfried Wilhelm Leibniz Prize) and by the European Union Horizon ERC-2012-SyG 318987 CToPAG. In addition, M.S.R. was supported by the Volkswagen Foundation (93 071) and the DFG (Projektnummer 329628492-SFB 1321 and INST 86/1800-1 FUGG). **Author contributions:** S.A.B., S.T., D.M., and S.B.N. initiated the project. S.A.B and S.B.N. designed experiments. S.B.N. performed mice experimental work, sample preparation, and bioinformatics analysis of data with the advice of and under the supervision of S.A.B. D.C. performed single-molecule mRNA FISH experiments and analysis. F.B. performed sample preparation, mass spectrometry experiments, and data processing under the supervision of M.S.R., who also did the proteomic data analysis and advised and supervised the evaluation of circadian analysis of both the transcriptomic and proteomic data. A.S. performed sleep analysis. L.O. performed data processing of transcriptomic data. M.M., supported and provisioned resources for the mass spectrometry experiments. S.B.N wrote the manuscript with editing input from M.S.R and S.A.B. **Data and materials availability:** RNA-seq data have been deposited in the ArrayExpress database at EMBL-EBI (www.ebi.ac.uk/arrayexpress) under accession number E-MTAB-7347. Images from the mRNA in situ have been deposited in the Zenodo repository (*72*). The mass spectrometry proteomics data have been deposited to the ProteomeXchange Consortium by means of the PRIDE partner repository with the dataset identifier PXD010697. Script for FISH image analysis is available at GitHub (https://github.com/dcolam/Cluster-Analysis-Plugin).

SUPPLEMENTARY MATERIALS

science.sciencemag.org/content/[vol]/[issue]/[elocator]/suppl/DC1
Figs. S1 to S12
Tables S1 to S9
References
View/request a protocol for this paper from *Bio-protocol*.

9 September 2018; accepted 3 September 2019
10.1126/science.aav2642